Zhang et al. Nanoscale Research Letters (2018) 13:237
https://doi.org/10.1186/s11671-018-2650-y

Nanoscale Research Letters

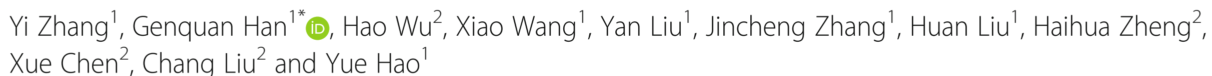

Reduced Contact Resistance Between Metal and n-Ge by Insertion of ZnO with Argon Plasma Treatment

Yi Zhang[1], Genquan Han[1*], Hao Wu[2], Xiao Wang[1], Yan Liu[1], Jincheng Zhang[1], Huan Liu[1], Haihua Zheng[2], Xue Chen[2], Chang Liu[2] and Yue Hao[1]

Abstract

We investigate the metal-insulator-semiconductor contacts on n-Ge utilizing a ZnO interfacial layer (IL) to overcome the Fermi-level pinning (FLP) effect at metal/Ge interface and reduce the barrier height for electrons. A small conduction band offset of 0.22 eV at the interface between ZnO and n-Ge is obtained, and the ZnO IL leads to the significant reduced contact resistance (R_c) in metal/ZnO/n-Ge compared to the control device without ZnO, due to the elimination of FLP. It is observed that the argon (Ar) plasma treatment of ZnO can further improve the R_c characteristics in Al/ZnO/n-Ge device, which is due to that Ar plasma treatment increases the concentration of oxygen vacancy V_o, acting as n-type dopants in ZnO. The ohmic contact is demonstrated in the Al/ZnO/n-Ge with a dopant concentration of 3×10^{16} cm^{-3} in Ge. On the heavily doped n$^+$-Ge with a phosphor ion (P$^+$) implantation, a specific contact resistivity of 2.86×10^{-5} Ω cm^2 is achieved in Al/ZnO/n$^+$-Ge with Ar plasma treatment.

Keywords: Germanium, Fermi-level pinning, Ohmic contact, Argon plasma, ZnO

Background

Germanium (Ge) has attracted much attention for the advanced metal-oxide-semiconductor field-effect transistors (MOSFETs) due to its higher carrier mobilities compared to Si [1, 2]. For the Ge p-channel MOSFETs, great progress has been made in growth of strained Ge channel [3–5], surface passivation [6–9], and source/drain (S/D) contacts [10], and the ultra-scaled Ge pFinFETs [11] have demonstrated the superior electrical performance to the Si devices. Ge n-channel transistors, by contrast, are still facing challenges, which produce the obstacle for the integration of Ge CMOS, including the poor interface quality, resulting in the low electron mobility, and the high S/D resistance due to the limited activation rate of n-type dopants in Ge [12] and the Fermi-level pinning (FLP) at metal/n-Ge interface [13]. FLP leads to a Schottky barrier height of about 0.5 eV for electrons for most of the metals on n-Ge, producing the very large contact resistance R_c [13–15].

Fermi-level depinning can be done by inserting a thin interfacial layer (IL), e.g., TiO_2 [16] and ZnO [17], between the metals and n-Ge [18], due to that the thin IL can block the metal wave function into Ge to reduce the metal-induced gap states [19, 20]. ZnO has small conduction band offset (CBO) with respect to Ge, which can lead to the smaller R_c in metal/ZnO/n-Ge, compared to metal/TiO_2/n-Ge with TiO_2/Ge having the positive CBO [16]. The dielectric constant of ZnO is smaller than that of TiO_2, so ZnO IL can obtain a thinner depletion region between the metal and n-Ge in comparison with TiO_2. In addition, it is easy to realize n-type doping in ZnO by introducing nonstoichiometric defects, such as oxygen vacancies V_o [21, 22], which gives rise to an even smaller ZnO depletion region between the metal and n-Ge. So far, in metal/ZnO/n-Ge contacts, the doping of ZnO by V_o was carried out by annealing in nitrogen atmosphere [16], which however, might resulted to the inter diffusion of ZnO and Ge during the annealing [23], and diffusion of dopant atoms in n-Ge during the annealing [24, 25], causing the degradation of current

* Correspondence: hangenquan@ieee.org; gqhan@xidian.edu.cn
[1]State Key Discipline Laboratory of Wide Band Gap Semiconductor Technology, School of Microelectronics, Xidian University, Xi'an 710071, People's Republic of China
Full list of author information is available at the end of the article

Springer Open
© The Author(s). 2018 **Open Access** This article is distributed under the terms of the Creative Commons Attribution 4.0 International License (http://creativecommons.org/licenses/by/4.0/), which permits unrestricted use, distribution, and reproduction in any medium, provided you give appropriate credit to the original author(s) and the source, provide a link to the Creative Commons license, and indicate if changes were made.

performance of the device. Since, a low-temperature process for depositing and doping ZnO needs to be developed.

In this work, we investigate the Fermi-level depinning at interface between metal and n-Ge by insertion of ALD deposited ZnO IL. The improvement effects of argon (Ar) plasma treatment of ZnO layer on contact resistance characteristics of Al/ZnO/n-Ge are studied.

Methods

Metal contacts were formed on both lightly and heavily doped n-Ge (001) wafers. The lightly doped Ge samples have a doping concentration about 3×10^{16} cm^{-3}. To achieve the heavily doped n-Ge, a phosphor ion (P^+) implant with a dose of 1×10^{15} cm^{-2} and an energy of 30 keV was performed on the n-Ge(001), which was followed by a rapid thermal annealing at 600 °C for 60 s. After wafer cleaning using several cycles of deionized water and diluted HCl, Ge wafers were immediately loaded into ALD (Beneq TSF-200) chamber to deposit ZnO, and then aluminum (Al) contacts were deposited by sputtering on Ge using a lift-off process. Here, three ZnO thicknesses of 1, 2, and 3 nm were utilized, which were confirmed by spectroscopic ellipsometry (SE) (J. A. Woollam M2000). During the ZnO deposition, diethyl zinc (DEZn) and deionized water (H_2O) were used as the Zn and O precursors, respectively, and the substrate temperature was kept 150 °C to eliminate the formation of GeO_x. The detailed ZnO deposition process using ALD was reported in our previous works in ref. [26, 27]. To further improve the conductivity of ZnO film, some ZnO on Ge samples were treated with argon (Ar) plasma. Control Al/n-Ge sample without ZnO IL was also fabricated. The R_c of Al on ZnO/Ge was extracted using the circular transmission line method (CTLM), which was formed by lift-off. The exposed ZnO was fully etched by plasma etch to ensure complete isolation between adjacent devices [16].

Keithley 4200 SCS was used to measure the electrical characteristics of the Al/ZnO/n-Ge contracts and CTLM structures, high-resolution transmission electron microscope (HRTEM) and X-ray photoelectron spectroscopy (XPS) were used to determine the microstructure and interface properties of the samples, and UV-VIS Spectrophotometer (LAMBDA 950, PerkinElmer) was used to determine the band gap E_g of deposited ZnO film.

Results and Discussion

Material Characterization of Al/ZnO/n-Ge

XPS valence band spectra of Ge/ZnO and transmittance spectrum of ZnO are presented in Figs. 1 and 2, respectively, which were utilized to investigate the mechanism of Fermi-level depinning effect at Al/ZnO/n-Ge interface. We conducted the XPS measurements for thick ZnO sample, ZnO/n-Ge interface sample, and pure Ge sample, to obtain the valence band offset (VBO) of ZnO/Ge, as shown in Fig. 1. The Zn 2*p* peak position and VBM for thick ZnO sample are 1021.9 eV and 2.59 eV, respectively. The Zn 2*p*

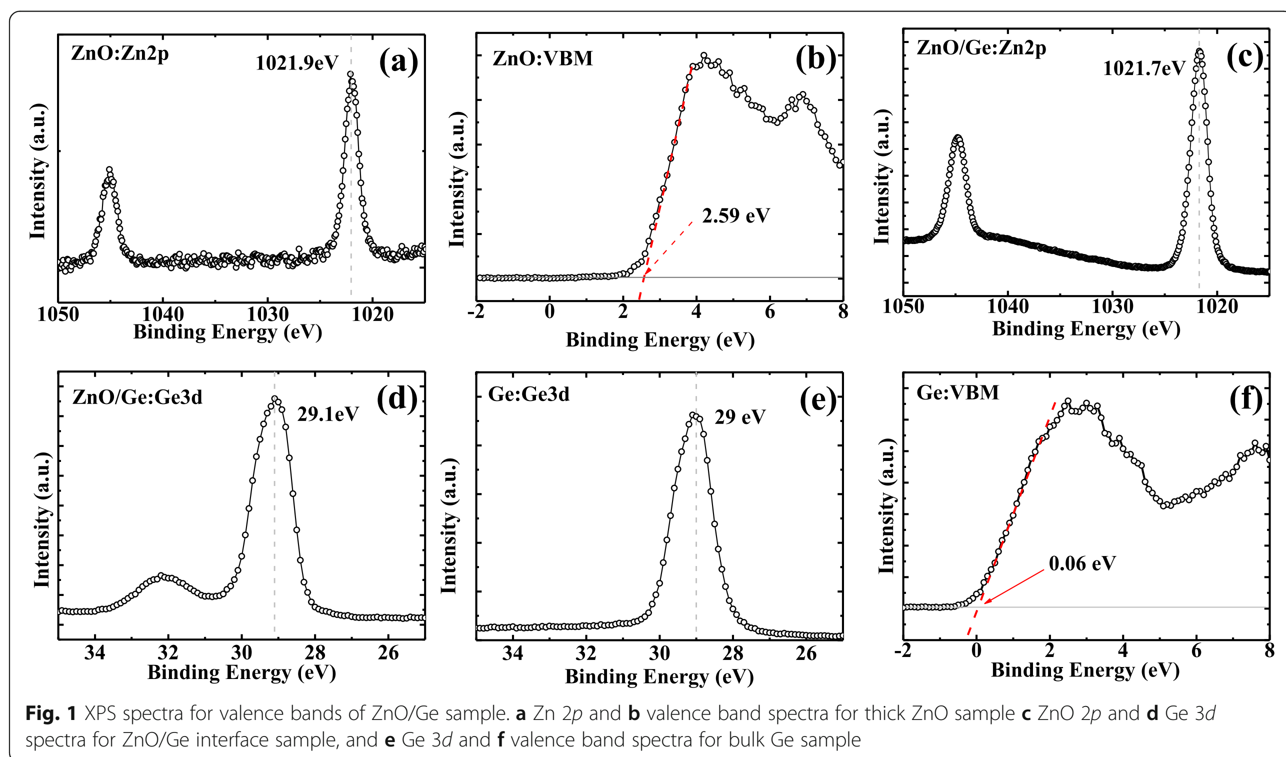

Fig. 1 XPS spectra for valence bands of ZnO/Ge sample. **a** Zn 2*p* and **b** valence band spectra for thick ZnO sample **c** ZnO 2*p* and **d** Ge 3*d* spectra for ZnO/Ge interface sample, and **e** Ge 3*d* and **f** valence band spectra for bulk Ge sample

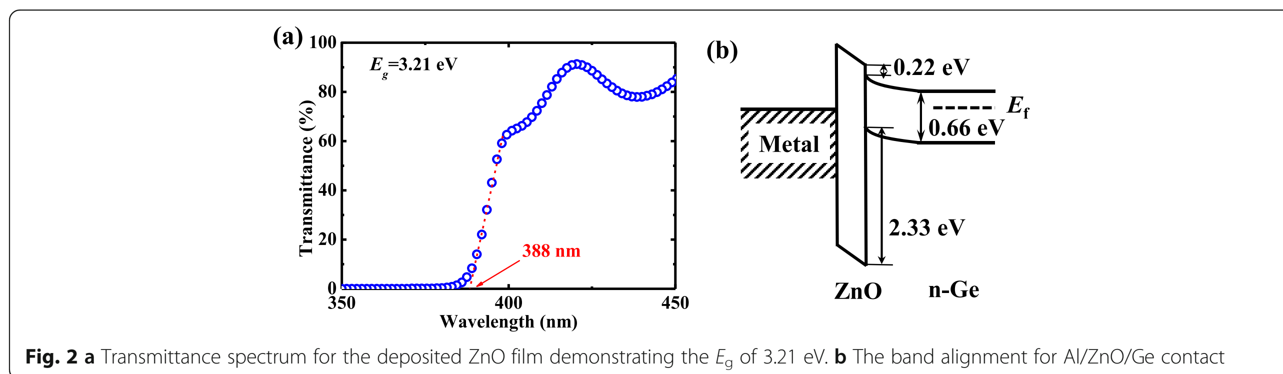

Fig. 2 **a** Transmittance spectrum for the deposited ZnO film demonstrating the E_g of 3.21 eV. **b** The band alignment for Al/ZnO/Ge contact

and Ge 3*d* peak position for ZnO/Ge interface sample are 1021.7 eV and 29.1 eV, respectively. The Ge 3*d* peak position and VBM for pure Ge sample are 29 eV and 0.06 eV, respectively. This indicates that the VBO of ZnO/Ge is 2.33 eV [30].

Figure 2a shows the transmittance plot obtained from UV-VIS spectroscopy for thick ZnO sample, and the E_g of ZnO is determined to be 3.21 eV, consistent with the reported values in [28, 29]. By using the obtained E_g of ZnO and VBO above, a CBO of 0.22 eV between ZnO and Ge is determined, as shown in Fig. 2b. This indicates that Fermi-level depinning can be achieved at Al/n-Ge interface using the ZnO insertion layer, which can produce the low R_c for Al/ZnO/n-Ge contact.

Figure 3 shows the TEM image of the Al/ZnO/n-Ge structure with the thickness of ZnO of 3 nm. A uniform and conformal ZnO layer is observed between Al and n-Ge. The inset in the top right corner illustrates the HRTEM image of zoomed-in view of the Al/ZnO/n-Ge interface. The thickness of ZnO film is measured to be 3 nm, which is consistent with result obtained by SE measurement, and the ZnO film is in an amorphous form.

A thin GeO_x interfacial layer is formed between Ge and ZnO, which is much smaller compared to [31] due to the lower deposition temperature used in this work. This is attributed to the fact that, during the deposition of ZnO, Ge reactive with O precursor, leading to the formation of GeO_x IL. GeO_x is also demonstrated by the XPS Ge 3*d* result in the inset in the top left corner.

Electrical conductivity of ZnO film can be improved by Ar plasma treatment, which causes the increasing in the concentration of oxygen vacancies V_o, acting as the donors in ZnO [32, 33]. Figure 4 depicts the XPS results of O 1*s* for as-deposited ZnO and the sample with Ar plasma treatment with a power of 50 W, an Ar gas flow of 60 sccm, and a duration of 45 s. The O 1*s* peak is deconvoluted into two peaks by using the Gaussian fitting. The peak at ~ 530 eV corresponds to lattice oxygen in ZnO [34, 35]. For the as-deposited sample, the peak at 531.7 eV corresponds to V_o (~ 531.5 eV) and chemisorbed oxygen on the surface of ZnO thin films, such as carbonyl and hydroxyl groups [35, 37]. For the sample with Ar plasma treatment, the peak is at ~ 531.5 eV, which shifts to lower binding energy, and gets much

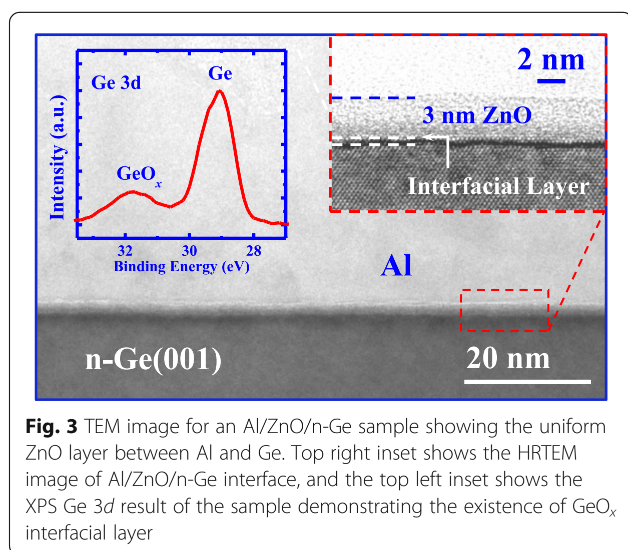

Fig. 3 TEM image for an Al/ZnO/n-Ge sample showing the uniform ZnO layer between Al and Ge. Top right inset shows the HRTEM image of Al/ZnO/n-Ge interface, and the top left inset shows the XPS Ge 3*d* result of the sample demonstrating the existence of GeO_x interfacial layer

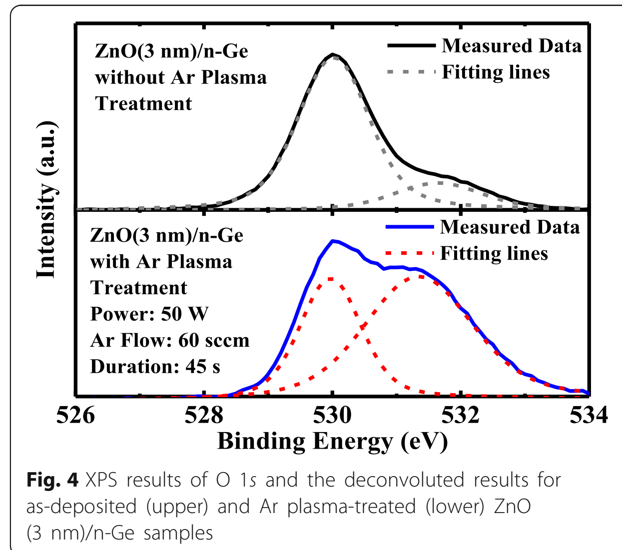

Fig. 4 XPS results of O 1*s* and the deconvoluted results for as-deposited (upper) and Ar plasma-treated (lower) ZnO (3 nm)/n-Ge samples

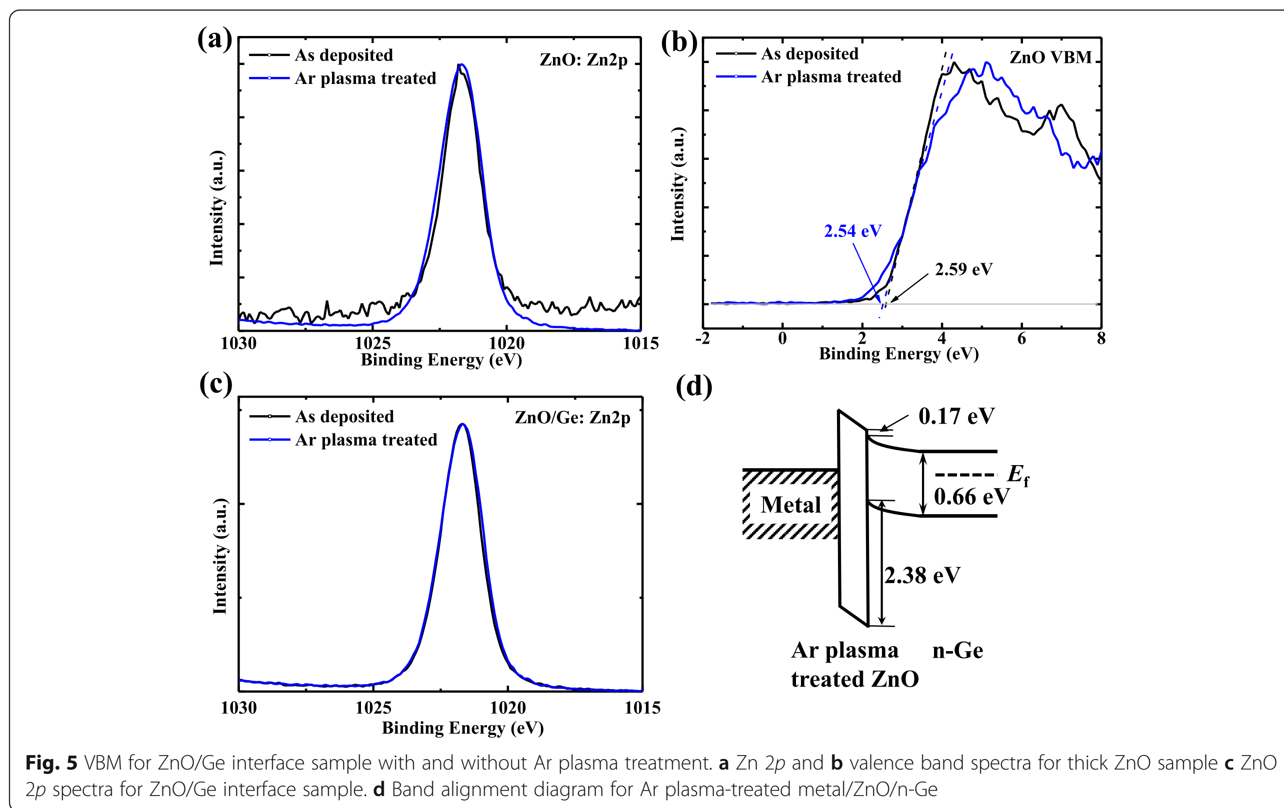

Fig. 5 VBM for ZnO/Ge interface sample with and without Ar plasma treatment. **a** Zn 2*p* and **b** valence band spectra for thick ZnO sample **c** ZnO 2*p* spectra for ZnO/Ge interface sample. **d** Band alignment diagram for Ar plasma-treated metal/ZnO/n-Ge

more pronounced in comparison with the as-deposited sample, indicating that more V_o are generated due to Ar plasma treatment, and chemisorbed oxygen is effectively removed. The increasing of n-type dopants in ZnO results in the thinner tunneling barrier and lower series resistance at interface, being responsible for the reduction in R_c [36].

We did the XPS measurements using thick ZnO sample and ZnO/Ge interface sample with and without Ar plasma treatment, as shown in Fig. 5. We found that, after Ar plasma treatment, there was a − 0.05 eV shift. This may indicate that the ZnO/Ge VBO is about 2.38 eV after Ar plasma treatment and CBO of 0.17 eV.

Electrical Performance of Al/ZnO/n-Ge Contacts

Figure 6a shows the measured current density *J* as a function of applied voltage *V* characteristics for Al contacts on lightly doped n-Ge. The Al/ZnO/n$^-$-Ge devices have the different thicknesses of ZnO layer. The schematic of the device is shown in the inset of Fig. 6.

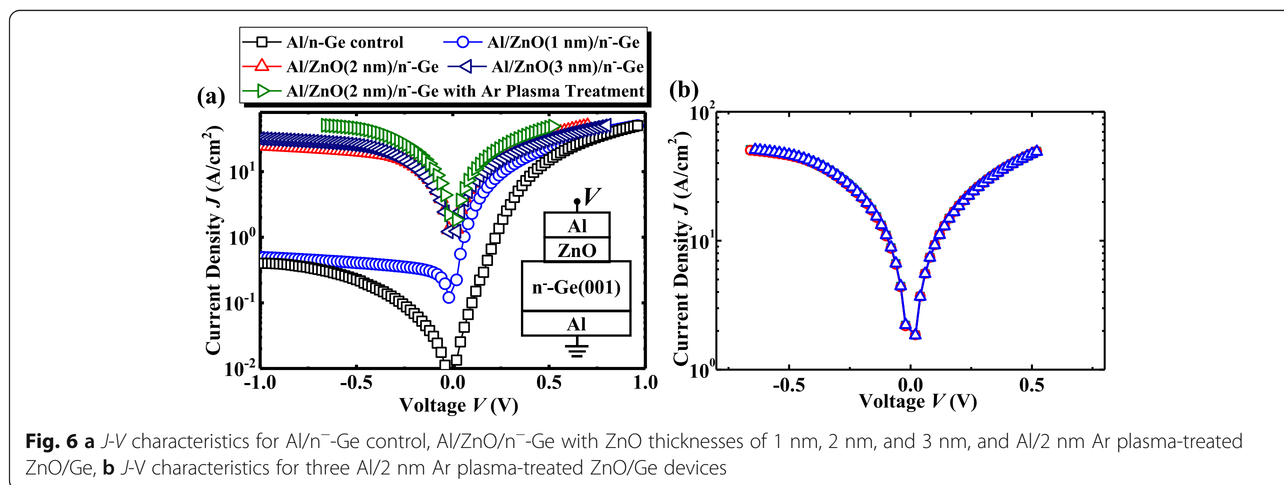

Fig. 6 a *J-V* characteristics for Al/n$^-$-Ge control, Al/ZnO/n$^-$-Ge with ZnO thicknesses of 1 nm, 2 nm, and 3 nm, and Al/2 nm Ar plasma-treated ZnO/Ge, **b** *J-V* characteristics for three Al/2 nm Ar plasma-treated ZnO/Ge devices

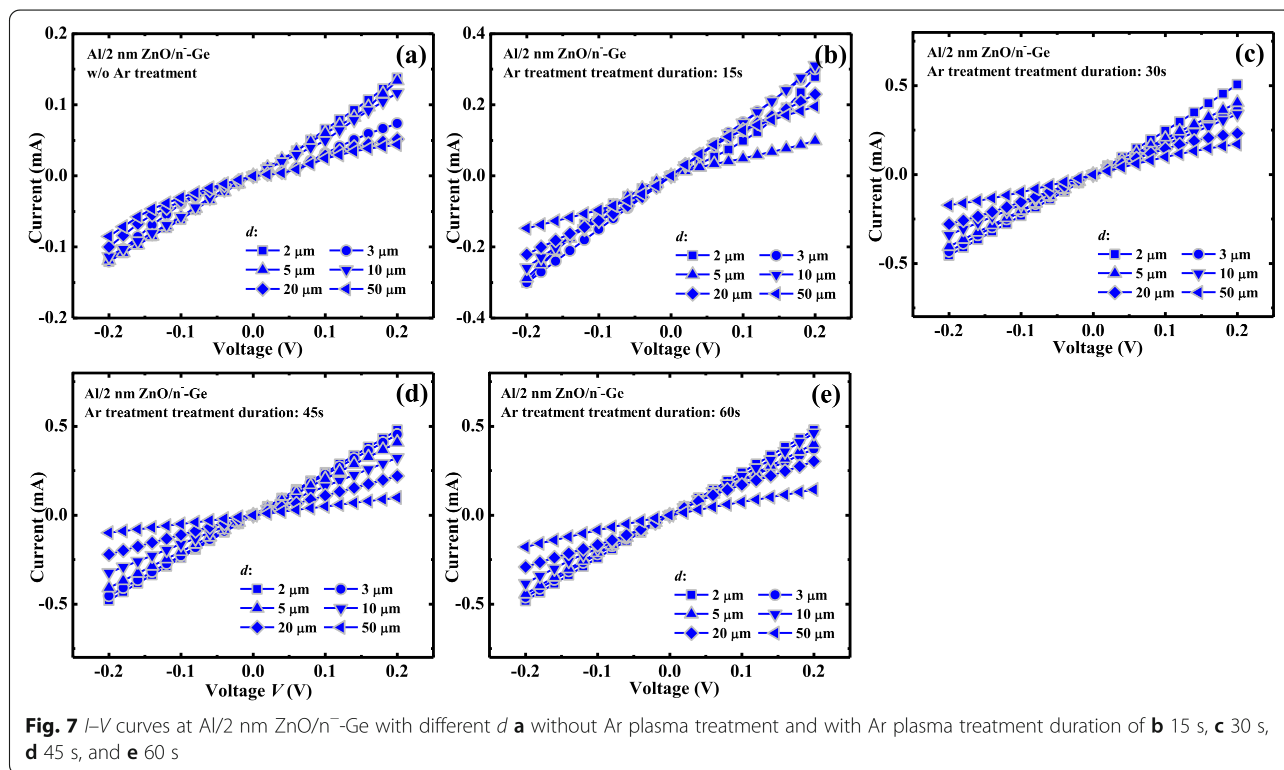

Fig. 7 *I–V* curves at Al/2 nm ZnO/n⁻-Ge with different *d* **a** without Ar plasma treatment and with Ar plasma treatment duration of **b** 15 s, **c** 30 s, **d** 45 s, and **e** 60 s

As predicted, the Al/n-Ge control device without ZnO shows the rectifying characteristics with the high barrier height for electrons due to the Fermi-level pinning at Al/n⁻-Ge [38]. Compared with the control Al/n-Ge sample without ZnO, Al/ZnO/n-Ge devices exhibit the improved reverse *J*, which is due to the Fermi-level depinning induced by the reduction of metal-induced-gap-states (MIGS) at metal/Ge interface [18, 19]. This improvement is more enhanced with thicker ZnO, which is due to the fact that more MIGS are eliminated. But the forward current density for 3 nm ZnO inserted device is smaller than that of 2 nm one. This may be explained as follows. The main current density for Al/ZnO/n-Ge is tunneling current. If the ZnO is not thick enough, MIGS will not be effectively eliminated, and it still shows rectifying characteristics. But if the ZnO is too thick, the series resistance of ZnO will dominate the whole resistance, and the current gets smaller. So there is a trade-off between elimination of MIGS and increase in series resistance of ZnO, and thus there is a critical thickness for the IL [19]. In conclusion, 2 nm is considered to be the optimal thickness for Al/ZnO/n-Ge contact.

With the Ar plasma treatment, the performance of Al/ZnO/n⁻-Ge device is further improved. Whatever for the reverse or forward sweeping of applied voltage *V*, Al/2 nm ZnO/n⁻-Ge device with Ar plasma

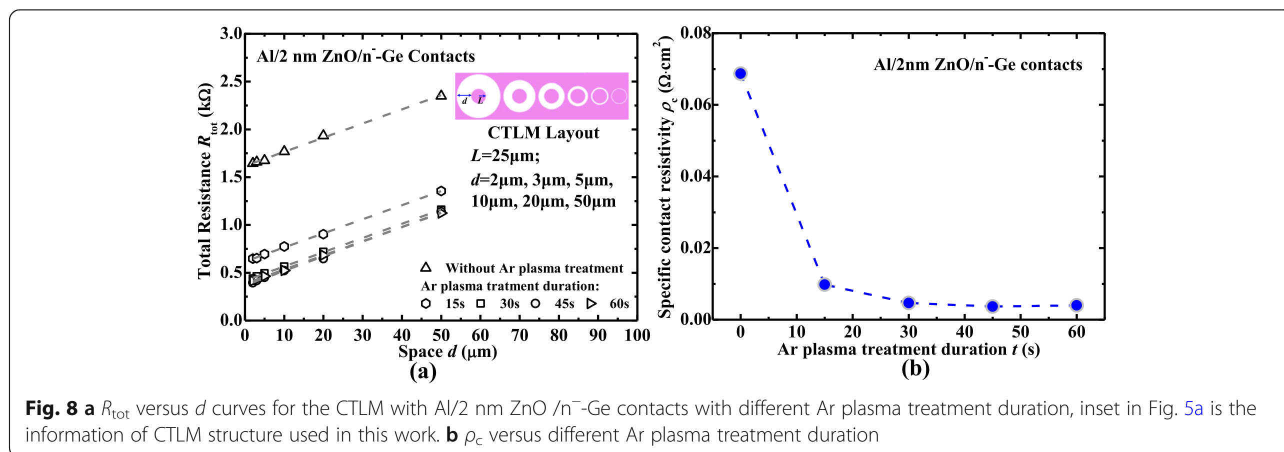

Fig. 8 **a** R_{tot} versus *d* curves for the CTLM with Al/2 nm ZnO /n⁻-Ge contacts with different Ar plasma treatment duration, inset in Fig. 5a is the information of CTLM structure used in this work. **b** ρ_c versus different Ar plasma treatment duration

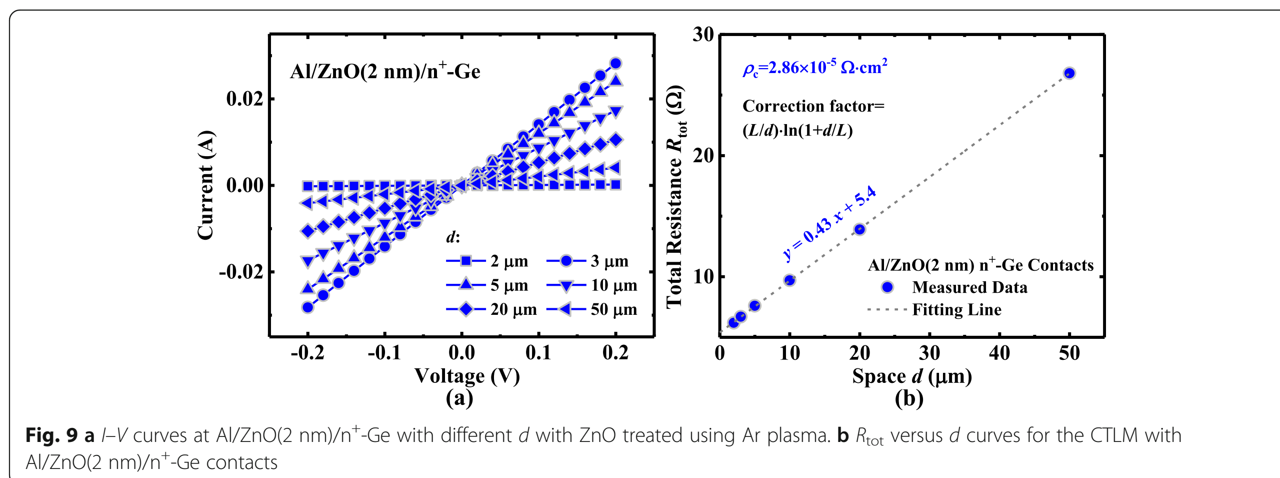

Fig. 9 a *I–V* curves at Al/ZnO(2 nm)/n$^+$-Ge with different *d* with ZnO treated using Ar plasma. **b** R_{tot} versus *d* curves for the CTLM with Al/ZnO(2 nm)/n$^+$-Ge contacts

treatment achieves the enhanced J compared to the device with 2 nm ZnO or 3 nm ZnO, which is due to that a large amount of V_o are generated in ZnO film during the Ar plasma treatment. The higher doping concentration in ZnO can effectively reduce the series resistance of ZnO and reduce the tunneling barrier for electrons at the interface between ZnO and Al, improving the tunneling current density.

Figure 6b shows *J-V* characteristics for three Al/2 nm ZnO/n$^-$-Ge device with Ar plasma treatment. It is clear that the J for different device is nearly the same, indicating that both ALD process and Ar plasma treatment have uniform effect on the improvement of current density.

Ohmic contacts are obtained for the Al/2 nm ZnO/n$^-$-Ge without and with different Ar plasma treatment duration of 15 s, 30 s, 45 s, and 60 s, respectively, which are shown in Fig. 7.

The raw total resistance R_{tot} between two contacts decreases with the decreasing of d, and the final R_{tot} is modified by a correction factor C, which is calculated with the equation $C = (L/d)\cdot\ln(1 + d/L)$ [39], where $L =$ 25 μm represents for the radius of inner pad, as depicted in the inset in Fig. 8a. By plotting the R_{tot} as a function of d in Fig. 8a, the sheet resistance R_{sh} of the n$^-$-Ge can be obtained from the line slope, and then ρ_c is calculated from the intercept of the linear fitting line with the vertical axis. For the Al/2 nm ZnO/n$^-$-Ge device without Ar plasma treatment, the ρ_c is 6.87×10^{-2} Ω cm^2, but after 45 s Ar plasma treatment, there is 17.2 times reduction compared with that without Ar plasma treatment and has the contact resistivity ρ_c of 3.66×10^{-3} Ω cm^2. We compare the values of ρ_c for the Al/2 nm ZnO/n$^-$-Ge devices with different Ar plasma treatment durations in Fig. 8b. It is observed that ρ_c of the device decreases with the treatment time up to 30 s. However, as treatment time is larger than 30 s, ρ_c nearly stays the same. The reduction in ρ_c may be attributed to the doping of ZnO, thus to the reduction of tunneling barrier and series resistance, as has mentioned previously. But there is no observable change in sheet resistance of n$^-$-Ge, indicating that there is no effect on the conductivity of n$^-$-Ge with Ar plasma treatment.

CTLM structure with Al contacts on heavily doped Ge is used to investigate the contact resistance characteristic of Al/2 nm ZnO/n$^+$-Ge. The ZnO layer underwent the Ar plasma treatment for 45 s. Figure 9a shows the measured *I-V* curves between the Al contacts with different d, showing the excellent ohmic performance. Figure 9b plots the R_{tot} as a function of d for Al/2 nm ZnO/n$^+$-Ge CTLM, and R_{sh} and ρ_c are extracted to be 64 Ω/□ and 2.86×10^{-5} Ω cm^2, respectively.

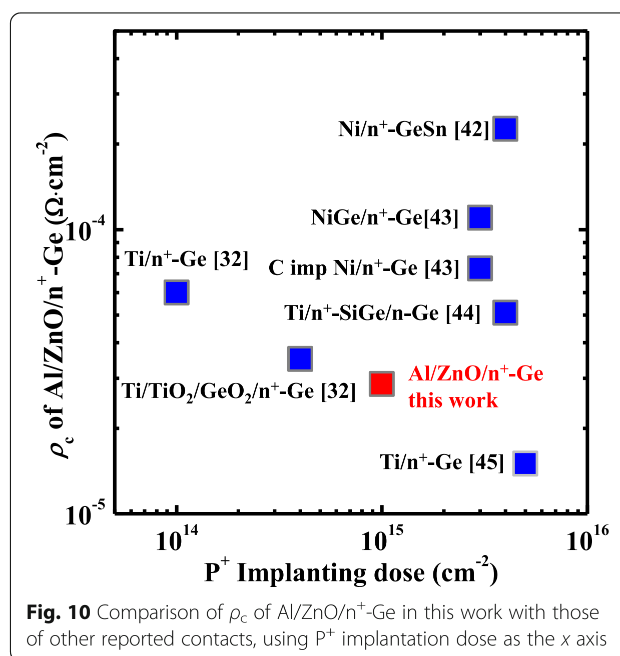

Fig. 10 Comparison of ρ_c of Al/ZnO/n$^+$-Ge in this work with those of other reported contacts, using P$^+$ implantation dose as the *x* axis

We compare the ρ_c of ZnO treated by Ar plasma Al/ZnO/n$^+$-Ge devices in this work with those reported in the literature, as shown in Fig. 10. For the heavily doped n$^+$-Ge contact sample, Al/ZnO/n$^+$-Ge contacts shown the smaller ρ_c in comparison with those of Ni/GeSn [40, 41], Ni/Ge [42], Ti/n$^+$-Ge in ref. [31], and Ti/TiO_2/GeO_2/Ge [31], carbon implanted Ni/Ge [42], and Ti/n$^+$-SiGe/n-Ge [43]. Metallic ohmic contacts such as Ni/Ge, Ni/GeSn, Ti/Ge, and carbon implanted Ni/Ge suffer from severe Fermi-level pinning, resulting in the large ρ_c. For Ti/TiO_2/GeO_2/Ge contact, a large tunneling resistance was introduced by the bilayer of 1 nm TiO_2/1.5 nm GeO_2 IL, degrading the contact resistivity characteristics. But the ρ_c in this work is larger than that in ref. [44]. We assume that this may due to the four times larger P$^+$ implantation dose than that in our work. Larger implantation dose will enable the heavier surface doping of n$^+$-Ge, resulting in the thinner Schottky barrier and smaller ρ_c. We believe that with heavier doping of n$^+$-Ge in Al/ZnO/n$^+$-Ge devices, smaller ρ_c will result in.

Conclusions

The Fermi-level depinning effect induced by ZnO IL in the Al/ZnO/n-Ge structures is investigated. XPS measurement demonstrated a small CBO of 0.22 eV at ZnO/n-Ge, i.e., elimination of FLP occurs, which leads to the ohmic metal contacts on n-Ge. It is further reported that Ar plasma treatment of ZnO leads to the increasing of concentration of V_o, acting as the n-type dopants in ZnO, which improves the R_c performance in Al/ZnO/n-Ge devices. Ohmic metal contacts are obtained on n$^-$ and n$^+$-Ge with the Ar plasma-treated ZnO IL. Based on the CTLM structures, values of ρ_c 3.66×10^{-3} Ω cm^2 and 2.86×10^{-5} Ω cm^2 are achieved in Al/2 nm ZnO/n$^-$-Ge and Al/2 nm ZnO/n$^+$-Ge, respectively, with the Ar plasma treatment of ZnO at a power of 50 W for 45 s.

Abbreviations

Al: Aluminum; ALD: Atomic layer deposition; Ar: Argon; CBO: Conduction band offset; CTLM: Circular transmission line method; DEZn: Diethyl zinc; E_g: Band gap; FLP: Fermi-level pinning; Ge: Germanium; GeO_x: Germanium oxide; GeSn: Germanium tin; HCl: Hydrochloric acid; HRTEM: High-resolution transmission electron microscope; IL: Interfacial layer; MIGS: Metal-induced-gap-states; MOSFETs: Metal-oxide-semiconductor field-effect transistors; Ni: Nickel; P$^+$: Phosphor ion; R_c: Contact resistance; R_{tot}: Raw total resistance; SE: Spectroscopic ellipsometry; Si: Silicon; Ti: Titanium; TiO_2: Titanium dioxide; UV-VIS: Ultraviolet–visible; VBO: Valence band offset; V_o: Oxygen vacancy; XPS: X-ray photoelectron spectroscopy; ZnO: Zinc oxide; ρ_c: Specific contact resistivity

Funding

The authors acknowledge the support from the National Key Research and Development Plan under Grant No. 2017YFB0403000, the National Natural Science Foundation of China under Grant Nos. 61534004, 61604112, and 61622405 and the founding of Jiangsu province under Grant No. BK20151250.

Availability of Data and Materials

The datasets supporting the conclusions of this article are included within the article.

Author's Contributions

YZ carried out the experiments and drafted the manuscript. GQH, YL, and JCZ supported the study and helped to revise the manuscript. HW and CL supported the deposition of ZnO. XW helped to revise manuscript. HL helped to carry out the measurements. HHZ and XC helped to deposit ZnO. YH provided constructive advice in the drafting. All the authors read and approved the final manuscript.

Competing Interests

The authors declare that they have no competing interests.

Publisher's Note

Springer Nature remains neutral with regard to jurisdictional claims in published maps and institutional affiliations.

Author details

[1]State Key Discipline Laboratory of Wide Band Gap Semiconductor Technology, School of Microelectronics, Xidian University, Xi'an 710071, People's Republic of China. [2]Key Laboratory of Artificial Micro- and Nano-structures of Ministry of Education, School of Physics and Technology, Wuhan University, Wuhan 430072, People's Republic of China.

Received: 10 March 2018 Accepted: 1 August 2018
Published online: 15 August 2018

References

1. Shang H, Schimdt HO, Chan KK, Copel M, Otto JA, Kozlowski PM, Steen SE, Cordes SA, Wong HSP, Jones EC, Haensch WE (2002) High mobility p-channel Ge MOSFETs with a thin Ge oxynitride gate dielectric. In IEDM Tech Dig:441–443. https://doi.org/10.1109/IEDM.2002.1175873
2. Wu N, Zhang Q, Chan DSH, Balasubramanian N, Zhu C (2006) Gate-first Germanium nMOSFET with CVD HfO_2/gate dielectric and silicon surface passivation. IEEE Electron Device Lett 27:479–481
3. Liu Y, Niu J, Wang H, Han G, Zhang C, Feng Q, Zhang J, Hao Y (2017) Strained germanium quantum well PMOSFETs on SOI with mobility enhancement by external uniaxial stress. Nanoscale Res Lett 12:120
4. Hashemi P, Chern W, Lee H, Teherani JT, Zhu Y, Gonsalvez J, Shahidi GG, Hoyt JL (2012) Ultrathin strained-Ge channel P-MOSFETs with high-K/metal gate and sub-1-nm equivalent oxide thickness. IEEE Electron Device Lett 33: 943–945
5. Pillarisetty R, Chu-Kung B, Corcoran S, Dewey G, Kavalieros J, Kennel H, Kotlyar R, Le V, Lionberger D, Metz M, Mukherjee N, Nah J, Rachmady W, Radosavljevic M, Shah U, Taft S, Then H, Zelick N, Chau R (2010) High mobility strained germanium quantum well field effect transistor as the p-channel device option for low power (V_{cc}= 0.5 V) III–V CMOS architecture. In IEDM Tech Dig:150–153. https://doi.org/10.1109/IEDM.2010.5703312
6. Zimmerman P, Nicholas G, Jaeger BD, Kaczer B, Stesmans A, Ragnarsson LÅ, Brunco DP, Leys FE, Caymax M, Winderickx G, Opsomer K, Meuris M, Heyns MM (2006) High performance Ge pMOS devices using a Si-compatible process flow. In IEDM Tech Dig:1–4. https://doi.org/10.1109/IEDM.2006.346870
7. Chui CO, Kim H, Chi D, Triplett BB, McIntyre PC, Saraswat KC (2002) A sub-400 °C germanium MOSFET technology with high-κ dielectric and metal gate. In IEDM Tech Dig:437–440. https://doi.org/10.1109/IEDM.2002.1175872
8. Kuzum D, Pethe AJ, Krishnamohan T, Oshima Y, Sun Y, McVittie JP, Saraswat KC (2007) Interface-engineered Ge (100) and (111), N-and P-FETs with high mobility. In IEDM Tech Dig:723–726. https://doi.org/10.1109/IEDM.2007.4419048
9. Takagi S, Takenaka M (2010) III-V/Ge CMOS technologies on Si platform. In VLSI-TSA Symp Tech Dig:147–148. https://doi.org/10.1109/ISSM.1995.524390
10. Li R, Lee SJ, Yao HB, Chi DZ, Yu MB, Kwong DL (2006) Pt-Germanide Schottky source/drain Germanium p-MOSFET with HfO2 gate dielectric and TaN gate electrode. IEEE Electron Device Lett 27:476–478
11. Duriez B, Vellianitis G, van Dal MJH, Doornbos G, Oxland R, Bhuwalka KK, Holland M, Chang YS, Hsieh CH, Yin KM, See YC, Passlack M, Diaz CH (2013) Scaled p-channel Ge FinFET with optimized gate stack and record performance integrated on 300 mm Si wafers. In IEDM Tech Dig:522–525. https://doi.org/10.1109/IEDM.2013.6724666

12. Chui CO, Gopalakrishnan K, Griffin PB, Plummer JD, Saraswat KC (2003) Activation and diffusion studies of ion-implanted p and n dopants in germanium. Appl Phys Lett 83:3275–3277
13. Nishimura T, Kita K, Toriumi A (2007) Evidence for strong Fermi-level pinning due to metal-induced gap states at metal/germanium interface. Appl Phys Lett 91:123123
14. Gallacher K, Velha P, Paul DJ, MacLaren I, Myronov M, Leadley DR (2012) Ohmic contacts to n-type germanium with low specific contact resistivity. Appl Phys Lett 100:022113
15. Nishimura T, Sakata S, Nagashio K, Kita K, Toriumi A (2009) Low temperature phosphorus activation in germanium through nickel germanidation for shallow n^+/p junction. Appl Phys Express 2:021202
16. Lin J, Roy A, Nainani A, Sun Y, Saraswat KC (2011) Increase in current density for metal contacts to n-germanium by inserting TiO_2 interfacial layer to reduce Schottky barrier height. Appl Phys Lett 98:092113
17. Manik P, Mishra R, Kishore V, Ray P, Nainani A, Yi H, Abraham M, Ganguly U, Lodha S (2012) Fermi-level unpinning and low resistivity in contacts to n-type Ge with a thin ZnO interfacial layer. Appl Phys Lett 101:182105
18. Roy AM, Jason Lin JY, Saraswat KC (2010) Specific contact resistivity of tunnel barrier contacts used for Fermi level depinning. IEEE Electron Device Lett 31:1077–1079
19. Gupta S, Manik P, Mishra R, Nainani A, Abraham M, Lodha S (2013) Contact resistivity reduction through interfacial layer doping in metal- interfacial layer-semiconductor contacts. J Appl Phys 113:234505
20. Dimoulas A, Tsipas P, Sotiropoulos A, Evangelou E (2006) Fermi-level pinning and charge neutrality level in germanium. Appl Phys Lett 89:252110
21. Kim HK, Han SH, Seong TY, Choi WK, Seong TY (2001) Electrical and structural properties of Ti/Au ohmic contacts to nZnO. J Electrochem Soc 148:G114
22. Li Y, Yao R, Wang H, Wu X, Wu J, Wu X, Qin W (2017) Enhanced performance in AZO based transparent flexible TFTs due to oxygen vacancy in ZnO film with Zn-Al-O interface fabricated by atomic layer deposition. ACS Appl Mater Inter 9:11711
23. Biswas D, Biswas J, Ghosh S, Wood B, Lodha S (2017) Enhanced thermal stability of Ti/TiO_2/n-Ge contacts through plasma nitridation of TiO_2 interfacial layer. Appl Phys Lett 110:052104
24. Koike M, Kamata Y, Ino T, Hagishima D, Tatsumura K, Koyama M, Nishiyama A (2007) Diffusion and activation of n-type dopants in germanium. J Appl Phys 104:023523
25. Ajmera AC, Rozgonyi GA, Fair RB (1987) Point defect/dopant diffusion considerations following preamorphization of silicon via Si^+ and Ge^+ implantation. Appl Phys Lett 52:813–815
26. Wang T, Wu H, Chen C, Liu C (2012) Growth, optical, and electrical properties of nonpolar m-plane ZnO on p-Si substrates with Al_2O_3 buffer layers. Appl Phys Lett 100:011901
27. Wang T, Wu H, Wang Z, Chen C, Liu C (2012) Ultralow emission threshold light-emitting diode of nanocrystalline ZnO/p-GaN heterojunction. IEEE Electron Device Lett 33:1030–1032
28. Elam D, Nemashkalo A, Strzhemechny Y, Chen C, Ayon A, Chabanov A (2011) Studies of optical and crystal properties of ALD grown ZnO. In: Design, Test, Integration and Packaging of MEMS/MOEMS (DTIP), 2011 Symposium on, pp 185–186
29. Iqbal J, Jilani A, Ziaul Hassan PM, Rafique S, Jafer R, Alghamdi AA (2016) ALD grown nanostructured ZnO thin films: effect of substrate temperature on thickness and energy band gap. J King Saud University – Science 28:347–354
30. Jia C, Chen Y, Guo Y, Liu X, Yang S, Zhang W, Wang Z (2011) Valence band offset of InN/$BaTiO_3$ heterojunction measured by X-ray photoelectron spectroscopy. Nanoscale Res Lett 6:316
31. Kim G, Kim S, Kim S, Park J, Seo Y, Cho B, Shin C, Shim J, Yu H (2016) Effective Schottky barrier height lowering of metal/n-Ge with a TiO_2/GeO_2 interlayer stack. ACS Appl Mater Inter 8:35419–35425
32. Vanheusden K, Seager CH, Warren WL, Tallant DR, Voigt JA (1996) Correlation between photoluminescence and oxygen vacancies in ZnO phosphors. Appl Phys Lett 68:403–405
33. Janotti A, Walle CGVD (2005) Oxygen vacancies in ZnO. Appl Phys Lett 87: 122102
34. Kim YH, Heo JS, Kim TH, Park S, Yoon MH, Kim J (2012) Flexible metal-oxide devices made by room-temperature photochemical activation of sol–gel films. Nature 489:128–132
35. Zhu Q, Xie C, Li H, Yang C, Zhang S, Zeng D (2014) Selectively enhanced UV and NIR photoluminescence from a degenerate ZnO nanorod array film. J Mater Chem C 2:4566–4580
36. Akazawa H (2009) Argon plasma treatment of transparent conductive ZnO films. Appl Phys Express 2:081601
37. Kim YJ, Yang BS, Oh S, Han SJ, Lee HW, Heo J, Jeong JK, Kim HJ (2013) Photobias instability of high performance solution processed amorphous zinc tin oxide transistors. ACS Appl Mater Inter 5:3255–3261
38. Yu H, Schaekers M, Barla K, Horiguchi N, Collaert N, Thean A, Meyer K (2016) Contact resistivities of metal-insulator-semiconductor contacts and metal-semiconductor contacts. Appl Phys Lett 108:171602
39. Martens K, Rooyackers R, Firrincieli A, Vincent B, Loo R, De Jaeger B, Meuris M, Favia P, Bender H, Douhard B, Vandervorst W, Simoen E, Jurczak M, Wouters DJ, Kittl JA (2011) Contact resistivity and Fermi-level pinning in n-type Ge contacts with epitaxial Si-passivation. Appl Phys Lett 98:023702
40. Kim G, Kim J, Kim S, Jo J, Shin C, Park J, Saraswat KC, Yu H (2014) Specific contact resistivity reduction through Ar plasma-treated TiO_{2-x} interfacial layer to metal/Ge contact. IEEE Electron Dev Lett 35:1076–1078
41. Zhang X, Zhang D, Zheng J, Liu Z, He C, Xue C, Zhang G, Li C, Cheng B, Wang Q (2014) Formation and characterization of Ni/Al ohmic contact on n^+-type GeSn. Solid State Electron 114:178–181
42. Duan N, Luo J, Wang G, Liu J, Simoen E, Mao S, Radamson H, Wang X, Li J, Wang W, Zhao C, Ye T (2016) Reduction of NiGe/n- and p-Ge specific contact resistivity by enhanced dopant segregation in the presence of carbon during nickel germanidation. IEEE Trans Electron Devices 63:4546–4549
43. Raghunathan S, Krishnamohan T, Saraswat KC (2010) Novel SiGe source/drain for reduced parasitic resistance in Ge NMOS. In: In ECS Meeting, pp 71–876
44. Chou CP, Chang HH, Wu YH (2018) Enabling low contact resistivity on n-Ge by implantation after Ti germanide. IEEE Electron Dev Lett 39:91–94

Submit your manuscript to a SpringerOpen journal and benefit from:

► Convenient online submission
► Rigorous peer review
► Open access: articles freely available online
► High visibility within the field
► Retaining the copyright to your article

Submit your next manuscript at ► springeropen.com